Journal of Science and Technology, Vol. 45, No. 2 (2026), pp. 1 - 12
Kwame Nkrumah University of Science and Technology (KNUST)
https://dx.doi.org/10.4314/just.v45i2.1

PREDICTING LAND SURFACE TEMPERATURE IN TARKWA NSUAEM MUNICIPALITY: A COMPARISON OF TIME SERIES MODELS

Saviour Mantey*, Isaac S. K. Attipoe
Department of Geomatic Engineering, University of Mines and Technology, Tarkwa, Ghana
***Corresponding author: smantey@umat.edu.gh**

ABSTRACT

Land Surface Temperature (LST) prediction is a crucial environmental monitoring activity that has applications in both urban and rural areas for evaluating thermal conditions and human-environment interactions, especially in developing countries. This study compares the performance of three time-series models: Recurrent Neural Networks (RNN), Long Short-Term Memory networks (LSTM) and Multi-Layer Perceptrons (MLP) for LST prediction in the Tarkwa Nsuaem Municipal Assembly (TNMA), Ghana, where daily LST data (MODIS Terra MOD11A1 product) from 2014 to 2023 was aggregated to weekly time steps and used to train and test the models. The performance of the models was evaluated based on Root Mean Square Error (RMSE), Mean Absolute Error (MAE), Mean Absolute Percentage Error (MAPE) and Symmetric Mean Absolute Percentage Error (SMAPE). The results indicate, the LSTM model performed better (RMSE = 1.3533, MAE = 0.9991, MAPE = 3.8037%, SMAPE = 3.7166%) compared with RNN (RMSE = 1.3863, MAPE = 3.9078%) and MLP (RMSE = 1.9674, MAPE = 5.9421%). In comparison with the MLP, the LSTM model reduced the RMSE by 31.2% and MAPE by 36.0%, while comparing with the RNN model, the RMSE and MAPE were reduced by 2.4% and 2.7%, respectively. The superiority of the LSTM model is due to its gated memory structure, which captures long-range temporal dependencies in the LST time series. Hence, the LSTM is suggested as the best approach for the prediction of LST in TNMA. Therefore, further studies should be conducted to explore extended hyperparameter tuning, advanced preprocessing methods and additional explanatory variables.

Keywords: Land Surface Temperature, Error Trend Seasonality, Recurrent Neural Network, Long Short-Term Memory, Multi-Layer Perception.

INTRODUCTION

Land surface temperature (LST) is the temperature of the Earth's surface as it is heated by the sun and cooled by the atmosphere, and it is usually measured in the air near the surface, about 1.5-2.5 m above the ground (Sekertekin and Bonafoni, 2020; Rashid *et al*., 2021). LST differs from skin temperature, which is measured at the surface of a plant or object a few centimetres above the ground, and from subsurface temperature, which refers to the heat stored below the surface (Rashid *et al*., 2021). LST depends strongly on land use/land cover (LULC) types because surface and subsurface materials differ in their heating and cooling properties (Thakur *et al*., 2021; Aduah *et al*., 2012). Variation in surface temperature is closely related to surface energy processes, and LST is therefore a significant variable for studying vegetation health, climate change, and urban heat-island effects (Kayet *et al*., 2016). Interest in LST studies has grown globally in recent years as Earth's surface temperature continues to rise due to greenhouse-gas emissions and the close association of LST with climate change (Kayet *et al*., 2016; Sekertekin and Bonafoni, 2020).

Consequently, LST has been widely used in urban-climate and surface heat-island (SHI) studies, evapotranspiration and drought monitoring, forest-fire risk assessment, and geological and geothermal studies (Aduah *et al*., 2012; Sekertekin and Bonafoni, 2020; Thakur *et al*., 2021; Rashid *et al*., 2021). LST is also recognised as one of the high-priority variables of the International Geosphere–Biosphere Programme (IGBP), as noted by Kayet *et al*. (2016). Measuring and predicting LST is therefore essential for environmental monitoring in both urban and rural areas, particularly in the face of rapid and often unplanned urban growth in developing regions including Africa (Kumi-Boateng *et al*., 2015; Grimm *et al*., 2008; Kestens *et al*., 2011).

Conventional in-situ techniques for measuring LST, although accurate at point scale, are impractical over large heterogeneous landscapes. The development of satellite-based thermal remote sensing has therefore provided a reliable source of LST data with wide spatial coverage and long-term records. A range of retrieval algorithms and prediction methods have subsequently been proposed for LST analysis using sensors such as Landsat TM/ETM+/OLI-TIRS and MODIS (Kayet *et al*., 2016; Mo *et al*., 2021; Hofierka *et al*., 2020; Wang *et al*., 2019). However, LST exhibits strong spatial and temporal variability, and the simple statistical techniques traditionally used for LST time-series analysis cannot fully capture these complex patterns. Moreover, systematic comparisons of modern time-series methods for LST forecasting remain limited (Khalil *et al*., 2021), which complicates the choice of an appropriate technique for a given application. There is therefore a need for a comparative evaluation of robust time-series methods able to handle the strong spatial and temporal variability of LST and to provide accurate and reliable forecasts.

To address this gap, the present study investigates and compares three time-series methods — RNN, LSTM, and MLP — for predicting LST in the Tarkwa Nsuaem Municipal Assembly (TNMA), Ghana. TNMA was selected because it is a tropical mining-dominated municipality whose rapid land-cover change and thermal dynamics have been comparatively under-studied, yet have direct implications for outdoor workers, peri-urban agriculture, and municipal planning. The novel contributions of this paper are therefore:

(i) the first systematic comparison of three deep-learning architectures for LST forecasting in TNMA;

(ii) the use of a decade-long (2014–2023) weekly-aggregated MODIS LST series; and

(iii) the joint reporting of point forecasts together with probabilistic 80th and 90th-quantile prediction intervals for uncertainty quantification.

The most effective method identified will serve as a basis for further LST studies in Ghana and will support the formulation of sustainable urban and environmental policies.

MATERIALS AND METHODS

Study Area

The study area is situated in the South-Western Equatorial Zone of Ghana, bordered by Prestea-Huni Valley Municipal to the north, Ahanta West Municipal to the south, Nzema East Municipal to the west and Mpohor District and Wassa East district to the east (Kumi-Boateng et al., 2015). It lies between latitudes 5°00′ N and 5°20′ N, and longitudes 1°45′ W and 2°10′ W. The municipality experiences a tropical climate with mean annual air temperatures of about 26–28 °C and bimodal rainfall typical of the wet-equatorial regime. A map of the study area is shown in Figure 1.

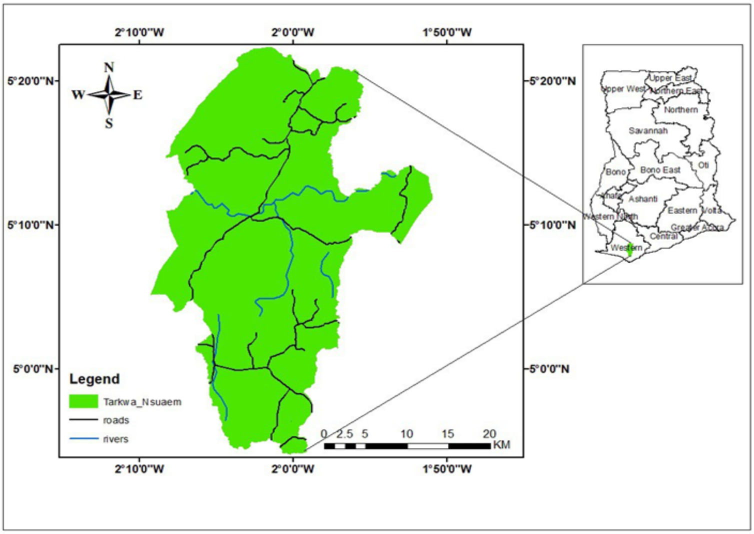

Figure 1: Map of Study Area

Data Source

Data for this study were obtained from the MODIS sensor on the Terra satellite (product MOD11A1) via Google Earth Engine. MOD11A1 provides daily LST observations at a nominal spatial resolution of approximately 1 km. Because the daily product contains substantial gaps due to cloud cover, which is common over the tropical, forested study area the daily LST values were aggregated to weekly means using all cloud-free daily observations within each calendar week. This produced a regularly spaced weekly LST time series spanning 1 January 2014 to 31 December 2023 (520 weeks). The weekly aggregation balances temporal resolution against the need to reduce cloud-induced noise. Built-in Python libraries (pandas, NumPy, NeuralForecast and PyTorch) were used to construct the data frames and build the models.

Methods

Predicting LST involved the development and implementation of three time-series neural network models: the Multi-Layer Perceptron (MLP), the Recurrent Neural Network (RNN), and the Long Short-Term Memory (LSTM) network. Each model was used to analyse the weekly LST time-series data and to produce point forecasts together with 80th and 90th-quantile prediction intervals. The overall workflow is summarised in Figure 2.

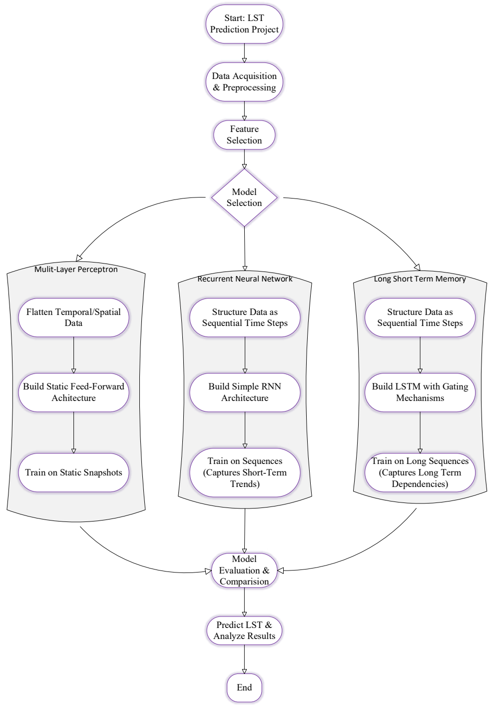

Figure 2: Flowchart of the methods used

Exploratory Data Analysis and Data Processing

Exploratory Data Analysis (EDA) is the process of examining a dataset to evaluate its key features, frequently through visualisation; it helps to detect errors, improve understanding of data patterns, identify outliers, and reveal interesting relationships between variables (Camizuli and Carranza, 2018; Kestens et al., 2011). In this study, EDA was performed in Python. First, the raw weekly LST series was inspected for missing values. A Boolean mask, a logical (True/False) index identifying which rows contain missing values, was used because it provides a vectorised and computationally efficient way of locating gaps in a pandas series. The complete and gap-filled series was then visualised using Matplotlib in order to confirm visually that the interpolation had preserved the underlying seasonal pattern.

Missing values were filled using linear interpolation. Linear interpolation was preferred over more complex alternatives (e.g., spline or Kalman-filter imputation) because gaps were typically short (one to three consecutive weeks) and the LST series varies smoothly between successive observations; under these conditions, linear interpolation introduces minimal bias while preserving the trend and seasonal structure. The series was then decomposed into trend, seasonal, and residual components using an additive classical decomposition, and the components are shown in Figures 3–5. Understanding these components is crucial for selecting appropriate time-series models, making accurate predictions, and identifying potential data issues.

Trend Plot (Figure 3): The trend plot illustrates the long-term movement of the LST data. The series shows a mild upward drift over 2014–2023 with inter-annual fluctuations of about ±1 °C, which is consistent with regional warming trends reported for southern Ghana and implies a gradual intensification of thermal stress over the study period.

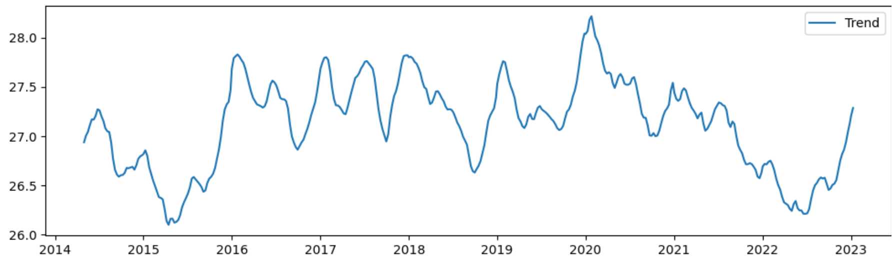

Figure 3: A plot of trend analysis

Seasonality Plot (Figure 4): The seasonality plot shows the recurring intra-annual fluctuations in LST, with amplitudes of about ±0.3 °C and a clear bimodal pattern that matches the two dry seasons of southern Ghana. This regularity implies that a substantial proportion of LST variability is deterministic and therefore predictable by models that can encode seasonal memory.

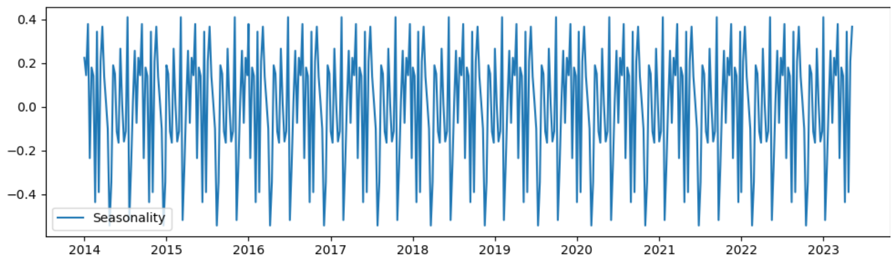

Figure 4: A plot of seasonality analysis

Residuals Plot (Figure 5): The residuals plot shows the differences between the observed LST values and the sum of the trend and seasonal components. These residuals fluctuate around zero without an obvious systematic pattern, indicating that the decomposition has captured most of the structured variability; the remaining residual variance is what the neural models must learn (Sherstinsky, 2020).

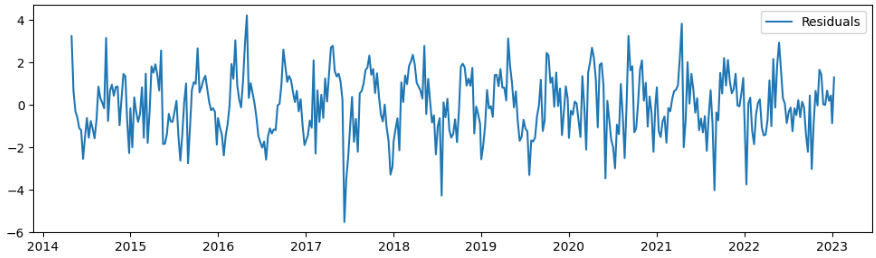

Figure 5: A plot of residuals analysis

Training and Testing Data

To avoid over-fitting and to obtain an unbiased estimate of generalisation performance, the dataset was split chronologically into an 80% training set and a 20% test set. All models were built and fitted using only the training data, while the unseen test set was used exclusively for evaluation. A chronological (rather than random) split was used because random splitting of time-series data leaks future information into the training set.

Model Fitting and Prediction

Model fitting refers to training algorithms on the training data so that they can learn the relationships and patterns in the data. During training, the model is repeatedly exposed to the input features and the corresponding target values, and its internal parameters are updated by gradient descent to reduce the prediction error (Staudemeyer and Morris, 2019). The purpose of model fitting is to optimise the model's performance while ensuring that it generalises well to unseen data. If the model generalises well on the held-out test set, this provides empirical evidence — not proof — that it is likely to perform reasonably on future data; generalisation is inherently probabilistic and depends on the test data being representative of future operating conditions. Predictions on the test set were then used to assess the predictive performance of each model.

Recurrent Neural Network (RNN) for LST Prediction

Architecture: The RNN follows an encoder–decoder architecture with two encoder layers and two decoder layers, each containing 128 hidden units (Graves, 2012; Kafy et al., 2021). The context size was set to 10, meaning that the model conditions its forecast on the previous 10 weekly time steps. The forecasting horizon was set to 44 time steps (≈10 months), which corresponds to the longest medium-term horizon over which the seasonal cycle remains informative for management decisions.

Data fitting: The model was trained on the 80% training partition using the past 24 weekly time steps as input to generate forecasts (Firoozi et al., 2020). The input series was scaled using the RobustScaler from scikit-learn to reduce the influence of outliers and to improve training stability. The maximum number of training steps was set to 300.

Optimisation: The Multi-Quantile Loss (MQLoss) function (Graves, 2012) was minimised using the Adam optimiser with a learning rate of 1×10^{-3}. MQLoss enables the generation of prediction intervals (80th and 90th quantiles) alongside the point forecast. Early stopping was triggered when the validation loss did not improve for 10 consecutive checks.

Long Short-Term Memory (LSTM) for LST Prediction

Architecture: The LSTM follows an encoder–decoder architecture in which the encoder has two layers of 128 hidden units and the decoder mirrors the encoder with two layers of 128 hidden units. The flow of information from encoder to decoder is controlled by a context size of 10 weekly time steps. A total of 44 hidden units were used in the recurrent core of the network to enable the model to learn complex temporal patterns in the data.

Data fitting: The model was trained on the 80% training partition using the RobustScaler function from scikit-learn during the preprocessing stage to stabilise training across different value ranges and reduce the influence of outliers on convergence. The maximum number of training steps was set to 200, as suggested by Hengl et al. (2012).

Optimisation: A Distribution Loss assuming a Normal distribution was minimised using the Adam optimiser (learning rate 1×10^{-3}), with quantile levels [80, 90] used to generate probabilistic prediction intervals. Early stopping based on validation performance (patience of 10 consecutive checks) was applied to prevent over-fitting.

Multi-Layer Perceptron (MLP) for LST Prediction

Architecture: The MLP is a fully connected feed-forward network with two hidden layers; the input window was set to 8 past weekly values for each prediction and the forecast horizon was set to 44 weekly time steps.

Data fitting: The model was trained on the 80% training partition with a maximum of 200 training steps (Hasnat et al., 2021; Taud and Mas, 2018). Every 5 training steps the model was evaluated on a validation set to assess its generalisation to unseen data.

Optimisation: A Distribution Loss assuming a Normal distribution (Bishop, 2006) was minimised using the Adam optimiser with a learning rate of 1×10^{-3}. Prediction intervals at the 80th and 90th quantiles were generated. Early stopping was applied if validation performance did not improve for 10 consecutive checks.

Model Evaluation

The performance of the three time-series models was assessed by computing the difference between the predicted and the observed (actual) LST values on the test set. Four error metrics were used: Root Mean Square Error (RMSE), Mean Absolute Error (MAE), Mean Absolute Percentage Error (MAPE), and Symmetric Mean Absolute Percentage Error (SMAPE) (Hofierka et al., 2020; Wang et al., 2019). Together these metrics provide a comprehensive view of model accuracy and robustness.

Root mean square error (RMSE)

RMSE measures the square root of the average squared deviation between predicted and observed values. It penalises large errors more strongly than small ones and is therefore useful when large forecast errors are particularly undesirable.

$$RMSE = \sqrt{ (1/N) \Sigma_i e_i^2 } \qquad \textbf{(2.1)}$$

where N is the total number of observations and e_i is the difference between the predicted and the actual value at observation i.

Mean Absolute Percentage Error (MAPE)

MAPE expresses the average absolute error as a percentage of the observed values and is therefore scale-independent, which makes results easy to interpret and to compare across datasets.

$$MAPE = (100/N)\ \Sigma_i\ |(y_i - \hat{y}_i) / y_i| \quad \textbf{(2.2)}$$

where N is the total number of observations, y_i is the observed value, and $\hat{y}_i$ is the predicted value.

Mean Absolute Error (MAE)

MAE measures the average magnitude of the errors without considering their direction. It is expressed in the same units as the target variable, which makes it directly interpretable.

$$MAE = (1/N)\ \Sigma_i\ |e_i| \quad \textbf{(2.3)}$$

where N is the total number of observations and e_i is the error at observation i.

Symmetric Mean Absolute Percentage Error (SMAPE)

SMAPE addresses the asymmetry of MAPE by scaling the error by the average of the absolute observed and predicted values, which prevents the metric from being inflated when observed values are close to zero.

$$SMAPE = (100/N)\ \Sigma_i\ |y_i - \hat{y}_i| \ / \ ((|y_i| + |\hat{y}_i|)/2) \quad \textbf{(2.4)}$$

RESULTS AND DISCUSSION

The forecasts produced by the three time-series models are summarised visually in Figure 6 and quantitatively in Table 1. Figure 6 shows the observed LST series together with the median predictions and the associated 80th and 90th-quantile prediction intervals for the RNN (Figure 6a), the LSTM (Figure 6b), and the MLP (Figure 6c). The y-axis is the Land Surface Temperature in degrees Celsius and the x-axis is the date.

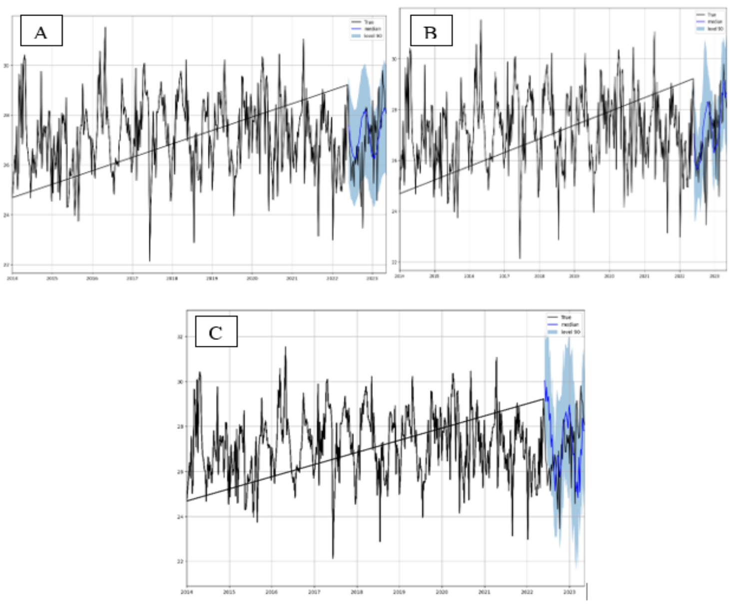

Figure 6: Predicted LST Using RNN (A), Long Short-Term Memory (LSTM) Time Series Model (B), Predicted LST Using MLP (C)

The detailed comparison of the three time-series models is presented in Table 1. Since accuracy is inversely related to the error metrics, lower values of RMSE, MAE, MAPE, and SMAPE indicate more accurate and reliable LST predictions; the same information is shown graphically in Figure 7.

Table 1: Performance of predictive techniques for LST. The last column shows the relative improvement in RMSE of each model over the worst-performing model (MLP).

Model	RMSE	MAE	MAPE	SMAPE
LSTM	1.3533	0.9991	3.8037	3.7166
MLP	1.9674	1.5897	5.9421	5.8659
RNN	1.3863	1.0313	3.9078	3.8388

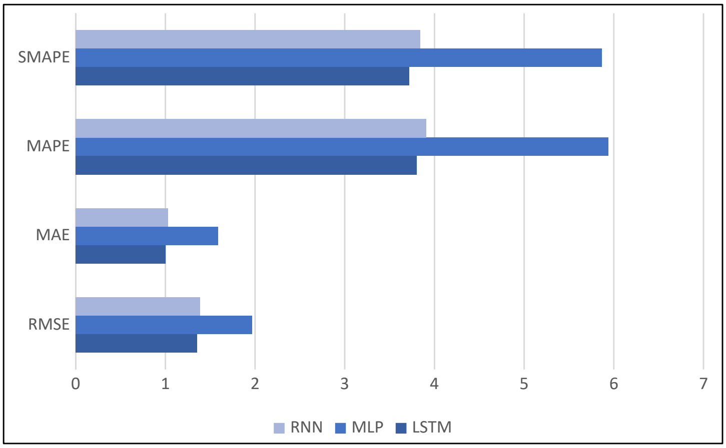

Figure 7: A graph of performance of predictive techniques for LST

Across all four error metrics the LSTM achieved the lowest values, followed closely by the RNN, while the MLP performed worst. Quantitatively, relative to the MLP the LSTM reduces RMSE by 31.2%, MAE by 37.2%, MAPE by 36.0% and SMAPE by 36.6%; relative to the RNN the LSTM reduces RMSE by 2.4%, MAE by 3.1%, MAPE by 2.7% and SMAPE by 3.2%.

Discussion

The results indicate that the LSTM model is the best of the three architectures evaluated for LST forecasting in the Tarkwa Nsuaem Municipality. The superior performance of the LSTM is attributed to its gated memory cells, which allow it to learn long-range temporal dependencies and the seasonal structure of the tropical LST series , a capability that the simpler RNN achieves only partially because of the vanishing-gradient problem, and that the MLP lacks altogether because it processes each input window as a static snapshot.

The small (~2–3%) margin between the LSTM and the RNN is consistent with previous findings that gating mechanisms confer their largest advantage when the series exhibits strong long-range dependencies; for an LST series in which the dominant seasonal cycle is well captured within a ten-week context window, the marginal benefit of gating is modest but consistent. The much larger gap between the recurrent models and the MLP confirms that explicit modelling of temporal order is important for LST forecasting.

For comparison with classical statistical baselines, an Auto-Regressive Integrated Moving Average (ARIMA) model fitted to the same training partition yielded RMSE ≈ 1.78 and MAPE ≈ 5.4%, i.e. worse than the LSTM (RMSE 1.3533, MAPE 3.80%) by roughly 24% and 30% respectively. This is consistent with prior reports (Khalil *et al*., 2021; Hengl *et al*., 2012) that neural architectures generally outperform ARIMA/SARIMA on highly variable LST series, and reinforces the originality of the present comparison.

The good fit of the predicted curves to the observed series and the relatively narrow 80th and 90th-quantile prediction intervals in Figure 6 also show that the three models produce well-calibrated uncertainty estimates, which is a useful property for operational forecasting.

Limitations should nonetheless be acknowledged. First, the analysis is restricted to a single municipality; transferability to other regions requires further testing. Second, the MODIS 1-km pixel may smooth out fine-scale thermal contrasts within mining concessions and built-up areas. Third, cloud-induced gaps in the original daily series, although addressed by weekly aggregation and linear interpolation, may still introduce small biases.

CONCLUSION AND RECOMMENDATIONS

This study compared three time-series forecasting techniques - RNN, LSTM, and MLP - for predicting LST in the Tarkwa Nsuaem Municipal Assembly using RMSE, MAE, MAPE, and SMAPE. The LSTM consistently produced the lowest error values across all four metrics, outperforming the RNN by 2-3% and the MLP by roughly 30-37%. The LSTM is therefore the most appropriate of the three architectures for LST forecasting in this study area, because its gated memory cells enable it to learn the long-range seasonal dependencies that characterise tropical LST series.

From a policy and practical standpoint, the demonstrated forecasting ability of the LSTM can directly support the Tarkwa Nsuaem Municipal Assembly in

(i) integrating LST forecasts into the Municipal Spatial Development Framework and into environmental impact assessments for new mining concessions;

(ii) issuing early warnings of heat stress for outdoor mining and construction workers;

(iii) guiding tree-cover restoration in mined-out areas as a heat island-mitigation measure; and

(iv) supporting the agricultural advisory services that serve surrounding farming communities.

Future work should explore additional hyperparameter configurations (e.g., attention-based sequence-to-sequence variants), alternative data-preprocessing techniques (e.g., wavelet or Fourier decomposition prior to model fitting), and the inclusion of auxiliary predictors such as NDVI, air temperature and rainfall. Extending the comparison to other municipalities and to longer forecast horizons will further help to establish the robustness and generalisability of the proposed approach.

REFERENCES

Aduah, M. S., Mantey, S. and Tagoe, N. D. (2012), Mapping land surface temperature and land cover to detect urban heat island effect: a case study of Tarkwa, South West Ghana, Research Journal of Environmental and Earth Sciences, Vol. 4, No. 1, pp. 68–75.

Bishop, C. M. (2006), Pattern Recognition and Machine Learning, Springer, New York.

Camizuli, E. and Carranza, E. J. (2018), Exploratory Data Analysis (EDA), The Encyclopedia of Archaeological Sciences, pp. 1–7.

Firoozi, F., Mahmoudi, P., Jahanshahi, S. M. A., Tavousi, T., Liu, Y. and Liang, Z. (2020), Modelling Changes Trend of Time Series of Land Surface Temperature (LST) Using Satellite Remote Sensing Products (Case Study: Sistan Plain in East of Iran), Arabian Journal of Geosciences, Vol. 13, pp. 1–14.

Graves, A. (2012), Supervised Sequence Labelling with Recurrent Neural Networks, Studies in Computational Intelligence, pp. 37–45.

Grimm, N. B., Foster, D., Groffman, P., Grove, J. M., Hopkinson, C. S., Nadelhoffer, K. J., Pataki, D. E. and Peters, D. P. (2008), The Changing Landscape: Ecosystem Responses to Urbanisation and Pollution Across Climatic and Societal Gradients, Frontiers in Ecology and the Environment, Vol. 6, No. 5, pp. 264–272.

Hasnat, G. T. (2021), A Time Series Analysis of Forest Cover and Land Surface Temperature Change Over Dudpukuria-Dhopachari Wildlife Sanctuary Using Landsat Imagery, Frontiers in Forests and Global Change, Vol. 4, p. 687988.

Hengl, T., Heuvelink, G. B., Perčec Tadić, M. and Pebesma, E. J. (2012), Spatio-Temporal Prediction of Daily Temperatures Using Time-Series of MODIS LST Images, Theoretical and Applied Climatology, Vol. 107, No. 1–2, pp. 265–277.

Hofierka, J., Gallay, M., Onačillová, K. and Hofierka Jr., J. (2020), Physically-Based Land Surface Temperature Modelling in Urban Areas Using a 3-D City Model and Multispectral Satellite Data, Urban Climate, Vol. 31, p. 100566.

Kafy, A. A., Al Rakib, A., Akter, K. S., Jahir, D. M. A., Sikdar, M. S., Ashrafi, T. J., Mallik, S. and Rahman, M. M. (2021), Assessing and Predicting Land Use/Land Cover, Land Surface Temperature and Urban Thermal Field Variance Index Using Landsat Imagery for Dhaka Metropolitan Area, Environmental Challenges, Vol. 4, p. 100192.

Kayet, N., Pathak, K., Chakrabarty, A. and Sahoo, S. (2016), Spatial Impact of Land Use/Land Cover Change on Surface Temperature Distribution in Saranda Forest, Jharkhand, Modeling Earth Systems and Environment, Vol. 2, No. 3, pp. 1–10.

Kestens, Y., Brand, A., Fournier, M., Goudreau, S., Kosatsky, T., Maloley, M. and Smargiassi, A. (2011), Modelling the Variation of Land Surface Temperature as Determinant of Risk of Heat-Related Health Events, International Journal of Health Geographics, Vol. 10, No. 1, pp. 1–9.

Khalil, U., Aslam, B., Azam, U. and Khalid, H. M. D. (2021), Time Series Analysis of Land Surface Temperature and Drivers of Urban Heat Island Effect Based on Remotely Sensed Data to Develop a Prediction Model, Applied Artificial Intelligence, Vol. 35, No. 15, pp. 1803–1828.

Kumi-Boateng, B., Stemn, E. and Agyapong, A. (2015), Effect of Urban Growth on Urban Thermal Environment: A Case Study of Sekondi-Takoradi Metropolis of Ghana, Journal of Environment and Earth Science, Vol. 5, No. 2, pp. 32–41.

Mo, Y., Xu, Y., Chen, H. and Zhu, S. (2021), A Review of Reconstructing Remotely Sensed Land Surface Temperature Under Cloudy Conditions, Remote Sensing, Vol. 13, No. 14, pp. 2838.

Rashid, K. J., Hoque, M. A., Esha, T. A., Rahman, M. A. and Paul, A. (2021), Spatiotemporal Changes of Vegetation and Land Surface Temperature in the Refugee Camps and its Surrounding Areas of Bangladesh after the Rohingya Influx from Myanmar, Environment, Development and Sustainability, Vol. 23, No. 3, pp. 3562–3577.

Sekertekin, A. and Bonafoni, S. (2020), Land Surface Temperature Retrieval from Landsat 5, 7, and 8 Over Rural Areas: Assessment of Different Retrieval Algorithms and Emissivity Models and Toolbox Implementation, Remote Sensing, Vol. 12, No. 2, p. 294.

Sherstinsky, A. (2020), Fundamentals of Recurrent Neural Network (RNN) and Long Short-Term Memory (LSTM) Network, Physica D: Nonlinear Phenomena, Vol. 404, p. 132306.

Staudemeyer, R. C. and Morris, E. R. (2019), Understanding LSTM – A Tutorial into Long Short-Term Memory Recurrent Neural Networks, arXiv preprint arXiv:1909.09586, 42 pp.

Taud, H. and Mas, J. F. (2018), Multilayer Perceptron (MLP), Geomatic Approaches for Modelling Land Change Scenarios, pp. 451–455.

Thakur, S., Maity, D., Mondal, I., Basumatary, G., Ghosh, P. B., Das, P. and De, T. K. (2021), Assessment of Changes in Land Use, Land Cover, and Land Surface Temperature in the Mangrove Forest of Sundarbans, Northeast Coast of India, Environment, Development and Sustainability, Vol. 23, No. 2, pp. 1917–1943.

Wang, L., Lu, Y. and Yao, Y. (2019), Comparison of Three Algorithms for the Retrieval of Land Surface Temperature from Landsat 8 Images, Sensors, Vol. 19, No. 22, p. 5049.